

Predictor Variable Prioritization in Nonlinear Models: A Genetic Association Case Study

Lorin Crawford^{1-3,†}, Seth R. Flaxman^{4,5}, Daniel E. Runcie⁶, and Mike West⁷

1 Department of Biostatistics, Brown University, Providence, RI, USA

2 Center for Statistical Sciences, Brown University, Providence, RI, USA

3 Center for Computational Molecular Biology, Brown University, Providence, RI, USA

4 Department of Mathematics, Imperial College London, London, UK

5 Data Science Institute, Imperial College London, London, UK

6 Department of Plant Sciences, University of California, Davis, CA, USA

7 Department of Statistical Science, Duke University, Durham, NC, USA

† Email: lorin_crawford@brown.edu

Abstract

The central aim in this paper is to address variable selection questions in nonlinear and nonparametric regression. Motivated within the context of statistical genetics, where nonlinear interactions are of particular interest, we introduce a novel and interpretable way to summarize the relative importance of predictor variables. Methodologically, we develop the “RelATive cEntrality” (RATE) measure to prioritize candidate predictors that are not just marginally important, but whose associations also stem from significant covarying relationships with other variables in the data. We focus on illustrating RATE through Bayesian Gaussian process regression; although, the methodological innovations apply to other and more general methods. It is known that nonlinear models often exhibit greater predictive accuracy than linear models, particularly for outcomes generated by complex architectures. With detailed simulations and a botanical QTL mapping study, we show that applying RATE enables an explanation for this improved performance.

1 Introduction

Classical statistical models and modern machine learning methodology have recently been dichotomized into two separate groups. The former are often characterized as interpretable modeling approaches and include conventional methods such as linear and logistic regressions. The latter, however, have sparked a greater debate as they have been frequently criticized as “black box” techniques with opaque implementations and uncertain internal workings. Whenever models, such as support vector machines or neural networks, give meaningful performance gains over more conventional regression methods, a challenge of explainability arises. To be more specific, it is often questioned what characteristics of the input data are being most used by the black box. One of the key features leading to these performance gains is the automatic inclusion of higher order interactions between variables (e.g. Cotter et al., 2011; Jiang and Reif, 2015). Popular machine learning kernel functions and fully connected neural network layers implicitly enumerate all possible nonlinear effects (e.g. Wahba, 1990). While this fact is in itself a partial explanation for improvement gains, we often wish to know precisely which variables are the most important — with the ultimate goals of furthering scientific understanding and performing model/feature selection (e.g. Barbieri and Berger, 2004).

As our main contribution, we propose a “RelATive cEntrality” measure (RATE) for investigating variable importance in Bayesian nonlinear models, particularly those considered to be black box. Here, RATE identifies covariates which are not just marginally important, but also those whose data associations stem from a significant covarying relationship with other variables. Our method is entirely general with respect to the modeling approach taken — the only requirement being that a method can produce uncertainty intervals for predictions. As an illustration, we focus on Gaussian process modeling with Markov chain Monte Carol (MCMC) inference; although, note that our variable selection approach immediately applies to other methodologies such as Bayesian neural networks (e.g. Richard and Lippmann, 1991), Bayesian additive regression trees (Chipman et al., 2010), and approximate inference methods like variational Bayes (e.g. Rasmussen and Williams, 2006).

While variable selection is the main utility for our method, we are motivated by the Bayesian modeling approach of continuous model expansion (e.g. Lakatos, 1980): the goal is to build the best fitting or optimally predictive model while searching over many variables and interactions, but without explicitly worrying about sparsity. Indeed, this has become a recent focus of statistical methods research, especially in terms of understanding relative importance of subsets of candidate predictors with respect to specific predictive goals (e.g. Lin et al., 2016). While we believe strongly in regularization as a key ingredient in developing good statistical models, we see this concept arise naturally and elegantly from our choice of modeling approach: we make use of Gaussian process priors, rather than explicitly imposing a sparsity penalty. The reason to avoid sparsity constraints like the lasso is not just philosophical — as typically applied L1-regularization suffers from a lack of stability (e.g. Lim and Yu, 2016; Piironen and Vehtari, 2017), and the use of Laplacian priors has too been criticized (e.g. Carvalho et al., 2010). Simultaneously, we are also motivated by the rise of deep neural networks, which are typically wildly over-parameterized and yet, when combined with large datasets, can give quite impressive improvements to model performance.

We assess our proposed approach in the context of statistical genetics, as a way to highlight data science applications that are driven by many correlated predictors. For example, understanding how nonlinear interactions or “epistasis” between genes influence the genetic architecture of traits and variation in phenotypes is of great interest in genetics applications (Mackay, 2014). However, despite studies that have detected pervasive epistasis in many model organisms (e.g. Horn et al., 2011) and improved phenotypic prediction using nonlinear regression models (e.g. Howard et al., 2014), substantial controversies remain (Hill et al., 2008). For example, in some settings, genetic mapping studies have identified many candidates of epistatic interactions that contribute to quantitative traits (e.g. Hemani et al., 2014), but some of these results can be explained by additive effects of other unsequenced variants (Wood et al., 2014). To date, our understanding of this important genetic question has been limited by the fact that it is often difficult to pinpoint how nonlinearities influence more complex prioritization of associated biological markers. Our contribution in this paper is therefore of direct scientific relevance in that RATE will enable scientists to consider embracing machine learning-type approaches by allowing them to open up the black box.

The remainder of this paper is organized as follows. In Section 2, we briefly detail the Gaussian process regression model and an effect size analogue that serves as a regression coefficient estimate for the original input covariates in nonparametric methods. In Section 3, we specify how to conduct variable selection using distributional centrality measures. Here, we also define the concept of relative centrality (RATE) which provides marginal evidence for the relative importance of each variable. In Section 4, we show the utility of our methodology on real and simulated data. Finally, we close with a discussion in Section 5.

2 Motivating Bayesian Nonparametric Framework

In this paper, we propose a relative centrality measure as an interpretable way to summarize the importance of input covariates for nonparametric methodologies. This effort will require the utilization of three components: (i) a motivating probabilistic model, (ii) a notion of an effect size (or regression coefficient) for each predictor variable, and (iii) a statistical metric that determines variable significance. Note that each of these components are naturally given in linear regression. Our goal is to provide a computationally tractable way to derive the same necessary components for nonlinear methods.

In this particular section, we focus on formulating components (i) and (ii). First, we begin by detailing Bayesian Gaussian process regression as our motivating probabilistic model. Next, we generalize a previous result which defines an effect size analogue for the input variables in nonparametric methods (Crawford et al., 2017). Extensions to other methodologies (e.g. Bayesian kernel ridge regression, neural networks) can be found in Supporting Information. For simplicity, we make the assumption that the targeted response variable is continuous; although, the frameworks discussed can be altered for dichotomous outcomes and binary classification problems. This expansion would include steps similar to those outlined in previous works (e.g. Zhang et al., 2011). We leave these specific details to the reader.

2.1 Gaussian Process Regression

We now state a Bayesian modeling framework which we use to construct a generalized projection operator between an infinite dimensional function space, called a reproducing kernel Hilbert space (RKHS), and the

original input covariate space. This projection will allow us to define an effect size analogue for Bayesian nonparametric analyses. We begin by considering standard linear regression

$$y = \mathbf{x}^\top \boldsymbol{\beta} + \varepsilon, \quad \varepsilon \sim \mathcal{N}(0, \tau^2), \quad (1)$$

where $y \in \mathcal{Y} \subseteq \mathbb{R}$ is a scalar quantitative response, $\mathbf{x} \in \mathcal{X} \subseteq \mathbb{R}^p$ is an input vector of predictor variables, $\boldsymbol{\beta}$ is a p -dimensional vector of regression coefficients (or effect sizes), and the residual noise ε is assumed to follow a univariate normal distribution with mean zero and variance τ^2 .

Note that in many practical applications, the assumption of a linear relationship between the covariates \mathbf{x} and their effect sizes $\boldsymbol{\beta}$ is too restrictive (e.g. Wahba, 1990; Rasmussen and Williams, 2006). One natural way to overcome this problem is to conduct model inference within a high dimensional function space. Indeed, an RKHS may be defined based on a nonlinear transformation of the data using a positive definite covariance (or kernel) function that is assumed to have a finite integral operator with eigenfunctions $\{\phi_i\}_{i=1}^\infty$ and eigenvalues $\{\delta_i\}_{i=1}^\infty$. Namely,

$$\int k(\mathbf{u}, \mathbf{v}) d(\mathbf{u}, \mathbf{v}) < \infty, \quad \delta_i \phi_i(\mathbf{u}) = \int_{\mathcal{X}} k(\mathbf{u}, \mathbf{v}) \phi_i(\mathbf{v}) d\mathbf{v}.$$

For these classes of covariance functions, the following infinite expansion holds $k(\mathbf{u}, \mathbf{v}) = \sum_{i=1}^\infty \delta_i \phi_i(\mathbf{u}) \phi_i(\mathbf{v})$ (Mercer, 1909), and an RKHS function space may be formally defined via the closure of a linear combination of basis functions (e.g. Pillai et al., 2007). As a direct result, we rewrite equation (1) as the following RKHS regression model (e.g. Zhang et al., 2011)

$$y = f(\mathbf{x}) + \varepsilon, \quad f(\mathbf{x}) = \boldsymbol{\psi}(\mathbf{x})^\top \mathbf{c}, \quad \varepsilon \sim \mathcal{N}(0, \tau^2), \quad (2)$$

where $\boldsymbol{\psi}(\mathbf{x}) = \{\sqrt{\delta_i} \phi_i(\mathbf{x})\}_{i=1}^\infty$ is a vector space spanned by the bases, $\mathbf{c} = \{c_i\}_{i=1}^\infty$ are the corresponding basis coefficients, and f is a function to be estimated. Notice that the above specification in (2) looks very much like the linear model in (1), except now the bases are $\boldsymbol{\psi}(\mathbf{x})$ (rather than the unit basis), and the transformed space can be infinite-dimensional. Theoretically, this is an important property because the inclusion of nonlinear relationships are implicitly captured in the RKHS; however, properly representing any given basis function in an empirically amenable form is difficult (Schölkopf et al., 2001).

To circumvent this analytical issue, one may alternatively conduct inference in an RKHS by specifying a Gaussian process to describe a prior distribution over the functions directly. Formally, this results in the rewriting of (1) as the following

$$y = f(\mathbf{x}) + \varepsilon, \quad f(\mathbf{x}) \sim \mathcal{GP}(m(\mathbf{x}), k(\mathbf{x}, \mathbf{x}')), \quad \varepsilon \sim \mathcal{N}(0, \tau^2), \quad (3)$$

where f is completely specified by its mean function and positive definite covariance (kernel) function, $m(\mathbf{x})$ and $k(\mathbf{x}, \mathbf{x}')$, respectively. In the practice, where there are a finite number of samples n , notice that there is modeling equivalence between (2) and (3). Moreover, if we condition on a finite set of locations, the Gaussian process prior then becomes a multivariate normal (e.g. Kolmogorov and Rozanov, 1960). By specifying a joint version of the nonparametric regression model above, we consider taking a “weight-space” view on Gaussian processes (Rasmussen and Williams, 2006),

$$\mathbf{y} = \mathbf{f} + \boldsymbol{\varepsilon}, \quad \mathbf{f} \sim \mathcal{N}(\mathbf{0}, \mathbf{K}), \quad \boldsymbol{\varepsilon} \sim \mathcal{N}(\mathbf{0}, \tau^2 \mathbf{I}), \quad (4)$$

where $\mathbf{y} = [y_1, \dots, y_n]^\top$ is now an n -dimensional response vector, \mathbf{I} is used to denote the identity matrix, and $\mathbf{f} = [f(\mathbf{x}_1), \dots, f(\mathbf{x}_n)]^\top$ is assumed to come from a multivariate normal with mean $\mathbf{0}$ and covariance matrix $\mathbf{K} = \boldsymbol{\Psi}^\top \boldsymbol{\Psi}$, where $k_{ij} = k(\mathbf{x}_i, \mathbf{x}_j)$ and $\boldsymbol{\Psi} = [\boldsymbol{\psi}(\mathbf{x}_1), \dots, \boldsymbol{\psi}(\mathbf{x}_n)]^\top$ is a corresponding matrix of concatenated basis functions. The key point here is that the form of (4) reduces an infinite-dimensional model fitting problem to just n -parameters. Altogether, we refer to the family of models taking on this form as Gaussian process (GP) regression.

Note that in many cases, the covariance function k is indexed by a bandwidth (also known as a smoothing parameter or lengthscale) h — which we expansively write as $k_h(\mathbf{u}, \mathbf{v})$. For example, the Gaussian kernel can be specified as $k_h(\mathbf{u}, \mathbf{v}) = \exp\{-\|\mathbf{u} - \mathbf{v}\|^2 / 2h^2\}$. Within a fully Bayesian model, this bandwidth parameter can be specified under a prior distribution and its posterior distribution may be inferred (e.g. Zhang et al., 2011). However for simplicity, we follow recent studies and work with a fixed bandwidth that we assume to be chosen as $h = \text{median}(\mathbf{D})$, where \mathbf{D} is a matrix of the euclidean measured distances between samples with $d(\mathbf{u}, \mathbf{v}) = \|\mathbf{u} - \mathbf{v}\|_2^2$ (e.g. Chaudhuri et al., 2017).

2.2 Nonlinear Projection onto Explanatory Variables

We now define the effect size analogue for general nonparametric methods (Crawford et al., 2017). We first briefly outline the conventional wisdom for coefficients in linear regression. In linear models, a natural interpretation of an effect size is the projection of the design matrix \mathbf{X} onto the response vector \mathbf{y} ,

$$\hat{\beta} = \text{Proj}(\mathbf{X}, \mathbf{y}), \quad (5)$$

with the choice of loss function, noise model, as well as prior distributions or regularization penalties, specifying the exact form of the projection. One standard projection operation is $\text{Proj}(\mathbf{X}, \mathbf{y}) = \mathbf{X}^\dagger \mathbf{y}$, where \mathbf{X}^\dagger is the Moore-Penrose generalized inverse — which, in the case of a full rank design matrix, equates to $\mathbf{X}^\dagger = (\mathbf{X}^\top \mathbf{X})^{-1} \mathbf{X}^\top$ and leads to the standard ordinary least-squares (OLS) regression coefficient estimates. For Bayesian procedures, priors over the parameters β induce a distribution on the projection procedure $\text{Proj}(\mathbf{X}, \mathbf{y})$ (e.g. Liang et al., 2008; Carvalho et al., 2010).

The general definition for the effect size analogue is based on the similar idea of projecting a nonlinear function onto the design matrix. Specifically, consider a nonlinear function evaluated on n -observed samples, such that $\mathbb{E}(\mathbf{y} | \mathbf{X}) = \mathbf{f}$. We formally define the *effect size analogue* as the result of projecting the design matrix \mathbf{X} onto the nonlinear response vector \mathbf{f} ,

$$\tilde{\beta} = \text{Proj}(\mathbf{X}, \mathbf{f}). \quad (6)$$

Note that this projection operation, and its practical calculation, effectively requires two sets of coefficients: (i) the theoretical coefficients \mathbf{c} on the basis functions; and (ii) the coefficients that determine the effect size analogue $\tilde{\beta}$. Following the formulation in equation (6), we use (2) and (4) to specify the joint projection of $\mathbf{f} = \Psi^\top \mathbf{c}$ onto the design matrix \mathbf{X} as the linear map,

$$\tilde{\beta} = \mathbf{X}^\dagger \Psi^\top \mathbf{c}. \quad (7)$$

The argument for why $\tilde{\beta}$ is an effect size analogue for nonparametric regression models is that, on the n -observations, $\mathbf{f} \approx \mathbf{X}\tilde{\beta}$. Additionally, the only requirement for (7) is a well-defined feature map $\psi(\mathbf{x})$. This includes taking the Cholesky decomposition of the covariance matrix as a feature map, or even employing low-rank approximations such as the Nystrom approximation (e.g. Drineas and Mahoney, 2005), random Fourier features (e.g. Rahimi and Recht, 2007), and explicit Mercer expansions (e.g. Fasshauer and McCourt, 2016). Importantly, the map from \mathbf{c} to $\tilde{\beta}$ is injective modulo the null space of the design matrix \mathbf{X} (Crawford et al., 2017). This is similar to the classical linear regression case where two different coefficient vectors will result in the same response estimate if the difference between the vectors is in the null space of \mathbf{X} . We should be clear that a variety of projection procedures (corresponding to various priors and loss functions) can be specified, and a systematic study elucidating which projections are efficient and robust is of interest for future research.

A key motivation for the effect size analogue is to conduct variable selection in the original input covariate space. When a response variable \mathbf{y} is solely driven by additive effects, the projections in (5) and (6) are equivalent, and the resulting effect size analogue from (7) is the same as the OLS estimate derived by a standard linear model. Furthermore, it has been shown (via Taylor series expansions) that certain covariance functions enumerate nonlinear effects among covariates (e.g. Jiang and Reif, 2015). The Gaussian kernel, in particular, includes all higher-order interaction components between predictor variables, where the contribution of the terms decays polynomially with the order of nonlinearity (e.g. Cotter et al., 2011). Therefore, when a response variable \mathbf{y} is driven by an arbitrary combination of additivity and interactions, a properly chosen nonlinear map $\psi(\mathbf{x})$ will lead to each $\tilde{\beta}_j$ equating to a weighted sum of higher order interactions between the j -th predictor and all other variables. We illustrate these concepts via simple simulation studies in the next two subsections.

Posterior Inference and Sampling. We now briefly detail a simple Markov chain Monte Carlo (MCMC) sampling procedure for estimating the implied posterior distribution of the effect size analogue. Once again, assume that we have the following conjugate hierarchical Gaussian process regression model

$$\mathbf{y} = \mathbf{f} + \varepsilon, \quad \mathbf{f} \sim \mathcal{N}(\mathbf{0}, \mathbf{K}), \quad \tau^2 \sim \text{Scale-Inv-}\chi^2(a, b), \quad \varepsilon \sim \mathcal{N}(\mathbf{0}, \tau^2 \mathbf{I})$$

where in addition to previous notation, we further assume that the residual variance parameter τ^2 follows a scaled-inverse chi-square distribution with degrees of freedom a and scale b as hyper-parameters. Given the conjugacy of this model specification, we may use a Gibbs sampler to estimate the joint posterior distribution $p(\mathbf{f}, \tau^2 | \mathbf{y})$. This consists of iterating between the following two conditional densities:

- (1) $\mathbf{f} | \tau^2, \mathbf{y} \sim \mathcal{N}(\mathbf{m}^*, \mathbf{V}^*)$ where $\mathbf{m}^* = \mathbf{K}(\mathbf{K} + \tau^2 \mathbf{I})^{-1} \mathbf{y}$ and $\mathbf{V}^* = \mathbf{K} - \mathbf{K}(\mathbf{K} + \tau^2 \mathbf{I})^{-1} \mathbf{K}$;
- (2) $\tau^2 | \mathbf{f}, \mathbf{y} \sim \text{Scale-Inv-}\chi^2(a^*, b^*)$ where $a^* = a + n$ and $b^* = a^{*-1}[ab + (\mathbf{y} - \mathbf{f})^\top (\mathbf{y} - \mathbf{f})]$;
- (3) $\tilde{\boldsymbol{\beta}} = \mathbf{X}^\dagger \mathbf{f}$.

Notice that the last step of the algorithm is deterministic and maps back to the effect size analogues. Iterating the above procedure T times results in a set of posterior draws: $\{\mathbf{f}^{(t)}, \tau^{2(t)}, \tilde{\boldsymbol{\beta}}^{(t)}\}_{t=1}^T$.

When considering an explicit basis function, using the effect size analogue simplifies Bayesian nonparametric predictive procedures to similar steps utilized by parametric methods (Crawford et al., 2017). Suppose that we have an $(n \times p)$ -dimensional out of sample test set \mathbf{X}^* and our goal is to determine the posterior predictive distribution of the vector \mathbf{y}^* . Here, samples may simply be drawn from the target distribution as $\{\mathbf{y}^{*(t)} = \mathbf{X}^* \tilde{\boldsymbol{\beta}}^{(t)}\}_{t=1}^T$. This differs from the way that posterior predictive intervals are computed in standard nonparametric models — as now quantiles and means only depend on the initial covariance matrix evaluated at the initial training data.

2.3 Simulations: Simple Illustration of the Effect Size Analogue

In this subsection, we use a simple simulation to illustrate the relationship between the conventional effect size $\hat{\boldsymbol{\beta}}_{\text{OLS}}$ and the nonlinear analogue for nonparametric regression methods $\tilde{\boldsymbol{\beta}}$. To do this, we use a simulated design matrix \mathbf{X} with $n = 500$ samples and $p = 4$ independent covariates to create continuous outcomes under a generative model taking on the form: $\mathbf{y} = \mathbf{X}\boldsymbol{\beta} + (\mathbf{x}_1 \circ \mathbf{x}_2)\gamma + \boldsymbol{\varepsilon}$, with $\boldsymbol{\varepsilon} \sim \mathcal{N}(\mathbf{0}, \tau^2 \mathbf{I})$. Here, we set $\tau^2 = 0.1$ and use $\mathbf{x}_1 \circ \mathbf{x}_2 = [\mathbf{x}_{11}\mathbf{x}_{21}, \dots, \mathbf{x}_{1n}\mathbf{x}_{2n}]^\top$ to denote the element-wise interaction between the two vectors. We consider two different simulation scenarios. In Scenario I, we use a purely additive model involving all covariates, where $\boldsymbol{\beta} = [\beta_1, \beta_2, \beta_3, \beta_4] = [0.4, -0.3, 1.2, -0.2]$ and $\gamma = 0$. Scenario II utilizes a sparse regression model, where we assume that only the first two predictors are causal and interact, setting $\boldsymbol{\beta} = [\beta_1, \beta_2, \beta_3, \beta_4] = [0.1, 0.2, 0, 0]$ and $\gamma = 1.5$.

For 100 different simulated dataset replicates, we begin by fitting a standard GP regression model with a zero mean prior and Gaussian covariance function to make up the matrix \mathbf{K} . Posterior estimates of the function \mathbf{f} are obtained by using the previously outlined Gibbs sampler with 10,000 MCMC iterations and model hyper-parameters set to $a = 5$ and $b = 2/5$. As a direct comparison, we also fit a standard linear model to serve as a baseline. The idea here is that we want to clearly illustrate the behavior of the effect size analogue between randomly sampled datasets. In order to do this, within each iterative data generating run, we calculate the OLS estimates for each coefficient using the standard projection for the linear model. We then compare these values to the effect size analogue, which we compute by taking the mean of the sequentially transformed posterior draws of \mathbf{f} under the projection operation defined in (7) (see the Algorithmic Overview in Supporting Information for more details).

Overall numerical results are presented in Table 1, while assessment of model fit can be found in Supporting Information (see Figure S1). First, we consider the case where both the linear model and GP were fit without including any interaction terms in the design matrix \mathbf{X} . The corresponding OLS estimates and the posterior mean of the effect size analogue are almost identical (average correlation ≈ 1 ; see Figure S1). As expected, both methods accurately estimate the coefficients of all four covariates in the first scenario. In the second scenario, each model assigns the greatest coefficient magnitude to predictors \mathbf{x}_1 and \mathbf{x}_2 — which we know to be involved in an interacting pair. Again, we want to point out that this behavior occurs for both the OLS estimates and the effect size analogues.

To investigate this performance further, we also consider a special case where we augment the design matrix to include an interaction term between \mathbf{x}_1 and \mathbf{x}_2 , such that $\mathbf{X}^* = [\mathbf{X}; \mathbf{x}_1 \circ \mathbf{x}_2]$. Here, the linear model is fit with the new design matrix. The GP regression, on the other hand, is fit with the original covariance matrix \mathbf{K} and the effect size analogue is computed as $\tilde{\boldsymbol{\beta}} = \mathbf{X}^{*\dagger} \mathbf{f}$. This inclusion of an extra interaction term does not inhibit either of the models from accurately estimating the true coefficients in the first simulation scenario. More notably, in the second scenario, the inclusion of the additional interaction term allows both

the linear model and the nonlinear projection of the GP regression to accurately estimate the the sparse additive and nonlinear effect components. Overall, this small example shows that the basic interpretability of the effect size analogue is similar to linear regression models in simple limiting cases.

2.4 Simulations: Predictive Advantage of the Effect Size Analogue

Now that we have developed a simple intuition for the effect size analogue, we next explore its advantages in predictive analyses. Here, the goal is to motivate the desire to have a principled variable selection procedure for nonparametric (black box) methods. To do this, we consider a more complex simulation design that is often utilized in statistical genetics to dissect the nonlinear architecture underlying phenotypic traits. First, we assume that the predictor variables explain a fixed proportion $V_{\mathbf{x}}$ of the total variance in the response $V(\mathbf{y})$. We examine two values $V_{\mathbf{x}} = \{0.25, 0.75\}$, which correspond to simulation scenarios I and II, respectively. This parameter $V_{\mathbf{x}}$ can alternatively be described as a factor controlling the signal-to-noise ratio. Next, we use a simulated design matrix \mathbf{X} with $n = 500$ samples and $p = 250$ independent covariates to generate \mathbf{y} . From this data, we randomly choose $p^* = 30$ “causal” (or truly associated) variables that we classify into two distinct groups: (i) a set of 10 solely additive covariates, and (ii) a set of 20 nonlinearly behaving covariates. All causal predictors in the second group have additive effects and are also involved in pairwise interactions.

The linear effect sizes for all p^* associated variables are assumed to come from a standard uniform distribution or $\beta_j \sim \mathcal{U}(0, 1)$. Next, we create a separate matrix \mathbf{W} which holds all pairwise interactions between the group 2 causal covariates. These corresponding interaction effect sizes are also drawn as $\gamma_j \sim \mathcal{U}(0, 1)$. We scale both the additive and interaction effects so that collectively they explain a fixed proportion of $V_{\mathbf{x}}$. Namely, the additive effects make up $\rho\%$, while the pairwise interactions make up the remaining $(1 - \rho)\%$. Alternatively, the proportion explained by the first group is said to be $V(\mathbf{X}\beta) = \rho V_{\mathbf{x}}$, while the proportion detailed by the second group is given as $V(\mathbf{W}\gamma) = (1 - \rho)V_{\mathbf{x}}$. Once we obtain the final effect sizes for all causal predictors, we draw normally distributed random errors as $\varepsilon \sim \mathcal{N}(\mathbf{0}, \mathbf{I})$ to make up the remaining $(1 - V_{\mathbf{x}})\%$ of $V(\mathbf{y})$. Finally, response variables are then created by summing over all effects using the simulation model: $\mathbf{y} = \mathbf{X}\beta + \mathbf{W}\gamma + \varepsilon$.

We consider three simulation cases that depend on the parameter $\rho = \{0, 0.5, 1\}$. Intuitively, $\rho = \{0, 1\}$ represents the limiting cases where the outcome is driven by only interaction or additive effects, respectively. For $\rho = 0.5$, the additive and interaction effects are assumed to equally contribute to the total variance of the simulated response. In these simulations, we are interested in examining the power of the effect size analogue and its ability to facilitate out-of-sample prediction. We evaluate the predictive accuracy of the same two methods: (a) the effect size analogue computed via a standard GP regression model with a zero mean prior and a Gaussian covariance function, and (b) the OLS estimates computed by standard linear models. Mean squared error (MSE) and predictive correlation (r) are used to compare out-of-sample predictive accuracy. We also record the tabulated frequency for which a given method exhibits the lowest MSE and greatest predictive r , which we denote as $\text{Opt\%}_{\text{MSE}}$ and Opt\%_r , respectively. We analyze 100 different simulated datasets for each scenario $V_{\mathbf{x}}$ and case ρ . Note that for each iterative run, we randomly split the data into training data with 80% of the samples and a test set with the remaining 20%.

Overall numerical results for each case of ρ are presented in Table 2, and then further illustrated as boxplots in Figure S2 to show how the two methods perform while taking into account variability (see Supporting Information). The effect size analogue, under GP regression, outperforms the standard linear model OLS estimates in a majority of the simulation scenarios. This discrepancy is particularly obvious when there is a low signal-to-noise ratio (i.e. $V_{\mathbf{x}} = 0.25$), as well as when there are underlying interactions affecting the model (i.e. $\rho = \{0, 0.5\}$). Altogether, these results are both consistent with past studies regarding nonparametric models (e.g. Howard et al., 2014) and unsurprising given that the effect size analogue is computed as a direct projection from functions estimated in a nonlinear space.

3 Variable Selection using Distributional Centrality Measures

As previously discussed, one main interest in nonparametric models is the potential to improve predictive accuracy over parametric models. A relevant subsequent task is to then determine the select subset of variables that give rise to this improved predictive performance. Recall that the effect size analogue serves

as a nonlinear summary coefficient for each of the covariates in the original input space. However, since the explicit projection in (7) does not always guarantee a preserved mapping of sparse solutions (Crawford et al., 2017), we cannot directly use standard Bayesian quantities such as posterior inclusion probabilities (PIPs) or Bayes factors (BFs) to rank variables in order of their significance. Indeed, there are many approaches to compute marginal association statistics for covariates based on their corresponding effect size estimates (e.g. Barbieri and Berger, 2004; Stephens and Balding, 2009), but many of these techniques rely on arbitrary thresholding. More importantly, they also fail to take into account any significant underlying dependencies and covarying relationships between predictors.

Our main methodological innovation is now developed. We introduce an analogy to traditional Bayesian hypothesis testing for nonparametric regression methods: a *post-hoc* approach for association mapping via a series of “distributional centrality measures” using Kullback-Leibler divergence (KLD) (e.g. Goutis and Robert, 1998; Smith et al., 2006; Woo et al., 2015; Tan et al., 2017; Piironen and Vehtari, 2016, 2017; Alaa and van der Schaar, 2017). Our strategy will be to use the posterior samples of the effect size analogues to infer the relative covariance between predictor variables. This underlying correlation structure will then be systematically searched over to posit significant individual associations. We refer to this approach as computing the “RelATive cENTrality” of covariates, or RATE.

3.1 Kullback-Leibler Divergence

Typical questions in network studies simplify to the general issue of determining the “centrality” of nodes — the potential importance of individual components in relation to the other nodes in the entire network. When network relationships are modeled via multivariate distributions, this can be explored in various statistical ways. Assume here that we have a collection of deterministically computed samples from the implied posterior distribution of the effect size analogue $\tilde{\beta}$ via equation (7). One interpretable way to summarize (in a single measure) the influence/importance of covariate \mathbf{x}_j on the rest of the variables in \mathbf{X}_{-j} is via the computation of the KLD measuring the difference between $p(\tilde{\beta}_{-j} | \tilde{\beta}_j)$ and $p(\tilde{\beta}_{-j})$. Specifically, this is defined by solving the following integral

$$\text{KLD}(\tilde{\beta}_j) = \int_{\tilde{\beta}_{-j}} \log \left(\frac{p(\tilde{\beta}_{-j})}{p(\tilde{\beta}_{-j} | \tilde{\beta}_j)} \right) p(\tilde{\beta}_{-j}) d\tilde{\beta}_{-j}. \quad (8)$$

Note that the KLD is a non-negative quantity and, in this context, takes the value of zero if and only if $p(\tilde{\beta}_{-j} | \tilde{\beta}_j) = p(\tilde{\beta}_{-j})$. Equivalently, this means that the KLD is zero if and only if the posterior distribution of $\tilde{\beta}_{-j}$ is independent of the effect $\tilde{\beta}_j$. Therefore, the case for which $\text{KLD}(\tilde{\beta}_j) = 0$ may simply be interpreted as meaning that covariate \mathbf{x}_j is not a key explanatory variable relative to others. Otherwise, for any given conditioning value $\tilde{\beta}_j$, the divergence in (8) represents the information (i.e. entropy) change induced on the distribution of $\tilde{\beta}_{-j}$ — naturally varying as the conditioning value $\tilde{\beta}_j$ varies.

Closed Form Derivation under Approximate Normal Posteriors. For our case study and immediate applications, we are interested in efficient computation of KLD measures in order to address problems with increasingly large numbers of predictor variables and interactions. For these purposes and the rest of the paper, we therefore restrict attention to contexts in which we can assume an adequate normal approximation to the full joint posterior distribution of the p -dimensional effect size analogue $\tilde{\beta}$. Ongoing and future work is concerned with computational and numerical aspects of the more general context, while the methodological and applied advances enabled by our approach are well-highlighted under the normal posterior assumption.

Thus, we take the posterior for $\tilde{\beta}$ as (approximately) multivariate normal with an empirical mean vector μ and positive semi-definite covariance/precision matrices $\Sigma = \Lambda^{-1}$ estimated via simulation methods. Consider the case where we want to investigate the centrality or marginal importance of covariate \mathbf{x}_j . We may partition conformably as follows

$$\tilde{\beta} = \begin{pmatrix} \tilde{\beta}_j \\ \tilde{\beta}_{-j} \end{pmatrix}, \quad \mu = \begin{pmatrix} \mu_j \\ \mu_{-j} \end{pmatrix}, \quad \Sigma = \begin{pmatrix} \sigma_j & \sigma_{-j}^\top \\ \sigma_{-j} & \Sigma_{-j} \end{pmatrix}, \quad \Lambda = \begin{pmatrix} \lambda_j & \lambda_{-j}^\top \\ \lambda_{-j} & \Lambda_{-j} \end{pmatrix},$$

where $\tilde{\beta}_j$, μ_j , σ_j and λ_j are scalars; $\tilde{\beta}_{-j}$, μ_{-j} , σ_{-j} , and λ_{-j} are $(p-1)$ -dimensional vectors; and Σ_{-j} and Λ_{-j} are $(p-1) \times (p-1)$ positive definite, symmetric matrices. Under this partitioning, we know that the marginally $\tilde{\beta}_{-j} \sim \mathcal{N}(\mu_{-j}, \Sigma_{-j})$. Furthermore, we also know that, when conditioned on predictor \mathbf{x}_j , $p(\tilde{\beta}_{-j} | \tilde{\beta}_j)$ is a multivariate distribution with expectation and covariance

$$\mathbb{E}(\tilde{\beta}_{-j} | \tilde{\beta}_j) = \mu_{-j} + \theta_j(\tilde{\beta}_j - \mu_j), \quad \text{V}(\tilde{\beta}_{-j} | \tilde{\beta}_j) = \Lambda_{-j}^{-1},$$

where $\theta_j = -\Lambda_{-j}^{-1}\lambda_{-j}$ is a $(p-1)$ -dimensional vector. Inserting these probability density forms into (8), with some algebraic rearrangement, yields the following

$$\text{KLD}(\tilde{\beta}_j) = \frac{1}{2} \left[-\log(|\Sigma_{-j}\Lambda_{-j}|) + \mathbb{E}(\epsilon_{-j}^\top \Lambda_{-j} \epsilon_{-j}) - 2\mathbb{E}(\epsilon_{-j}^\top) \Lambda_{-j} \epsilon_j - \mathbb{E}(\epsilon_{-j}^\top \Sigma_{-j} \epsilon_{-j}) + \epsilon_j^2 \theta_j^\top \Lambda_{-j} \theta_j \right], \quad (9)$$

where $|\cdot|$ represents the matrix determinant, $\epsilon_{-j} = \tilde{\beta}_{-j} - \mu_{-j}$ is a matrix, $\epsilon_j = \tilde{\beta}_j - \mu_j$ is a scalar, and the expectations are taken with respect to the marginal posterior distribution of $\tilde{\beta}_j$. Next, denote the following definition of an expectation of quadratic forms (Mathai and Provost, 1992),

$$\mathbb{E}(\mathbf{u}^\top \mathbf{Q} \mathbf{u}) = \mathbb{E}(\mathbf{u}^\top) \mathbf{Q} \mathbb{E}(\mathbf{u}) + \text{tr}(\text{V}(\mathbf{u}) \mathbf{Q}),$$

for any vector \mathbf{u} and positive semi-definite covariance matrix \mathbf{Q} , where $\text{tr}(\cdot)$ is the matrix trace function. Using this equality, the computation of the KLD in (9) simplifies to the following closed form solution

$$\text{KLD}(\tilde{\beta}_j) = \frac{1}{2} \left[-\log(|\Sigma_{-j}\Lambda_{-j}|) + \text{tr}(\Sigma_{-j}\Lambda_{-j}) + 1 - p + \alpha_j(\tilde{\beta}_j - \mu_j)^2 \right], \quad (10)$$

where $\alpha_j = \theta_j^\top \Lambda_{-j} \theta_j = \lambda_{-j}^\top \Lambda_{-j}^{-1} \lambda_{-j}$ and $\text{tr}(\mathbf{I}) = p-1$. By symmetry in the notation for elements of sub-vectors and sub-matrices, it trivially follows that we may simply permute the order of the variables in $\tilde{\beta}$ and iteratively compute the KLD to measure the centrality of any predictor variable \mathbf{x}_j .

Prioritization and Relative Significance. In this particular context, values $\tilde{\beta}_j$ close to zero may be interpreted as “null hypotheses” of little to no relevance to the modeled outcome. Therefore, searching for the most central (i.e. influential) predictors simply reduces to looking for the greatest KLD when setting each $\tilde{\beta}_j = 0$. More contextually specific questions arise when deciding if a given centrality measure is significant. Indeed, in practice, a threshold may be chosen in order to determine if any given KLD represents a significant shift in entropy. Previous studies have done this through k -fold permutation to find an effective predictor-wide threshold (e.g. Woo et al., 2015). A more computationally efficient option for determining a natural ranked cutoff is to explore the relevance of variables recursively, and judge their significance via a scaled version of the KLD. We call this “RelATive cEntRality” or RATE,

$$\text{RATE}(\tilde{\beta}_j) = \text{KLD}(\tilde{\beta}_j) / \sum \text{KLD}(\tilde{\beta}_\ell), \quad \sum \text{RATE}(\tilde{\beta}_j) = 1. \quad (11)$$

Here, the RATE measure is bounded within the range $[0, 1]$, with the natural interpretation of measuring a variable’s relative importance. Suppose that \mathbf{x}_j identifies the covariate with the largest RATE value. Conditioning on a reduced margin, and then repeating the computation outlined in (10) and (11), will identify the relatively second most explanatory predictor. We can repeat this procedure until each of the remaining covariates appear to be equal in their relative importance. This would indicate that all significant predictors had been identified, and all that remain are variables for which their influences on the posterior distribution are indistinguishable. This recursive process can be simplified to defining an initial set of candidate associated variables with first order centrality measures satisfying

$$\{j : \text{RATE}(\tilde{\beta}_j) > 1/p\}.$$

The value $1/p$ represents the level at which there is relative equal importance across all predictors; and hence, there are no central nodes that exist within the posterior distribution. We may quantify this behavior by checking the entropic difference between a uniform distribution and the observed RATE measures. Namely,

$$\Delta = \log(p) - H, \quad H = - \sum \text{RATE}(\tilde{\beta}_j) \log(p \cdot \text{RATE}(\tilde{\beta}_j)), \quad (12)$$

where H represents the intrinsic entropy of the relative centrality measures, and the case of no significantly associated covariates yields an entropy of $\log(p)$. One way to calibrate Δ is linked to effective sample size (ESS) measures from importance sampling (Gruber and West, 2016, 2017). In a very different applied context, authors have exploited the use of an approximate ESS measure defined by

$$\text{ESS} = 1/(1 + \Delta) \times 100\%. \quad (13)$$

This ESS measure is a calibration metric that provides a notion of “loss in uniformity”. For example, 50% loss in terms of (1-ESS) translates to a larger Δ value of 1. This equates to the presence of at least one predictor that is significantly associated with the modeled response. On the other hand, a minor 5% loss corresponds to a more uniform case with Δ value of about 0.05. Again, this latter scenario would occur when there are hardly any influential covariates within the data.

For any given set of significant variables, according to their estimated RATE measure, further analyses may be carried out involving the relative costs of false positives and negatives to make an explicitly reasoned decision about which predictors to pursue (Stephens and Balding, 2009). Unless stated otherwise, the results we present throughout the rest of the paper will be based on using RATE. We explore the power of this alternative approach for determining variable significance in Section 4.

3.2 Relationship to Graphical Models and Precision Analysis

The proposed variable selection procedure is very much related to precision analysis. It follows that the rate of change for the Kullback-Leibler divergence (i.e. the first derivative of (10) with respect to a given effect size analogue), is found via the term $\alpha_j = \boldsymbol{\lambda}_{-j}^\top \boldsymbol{\Lambda}_{-j}^{-1} \boldsymbol{\lambda}_{-j}$. This means that the closed form computation of the KLD is directly impacted by the deviations between the approximation of a given predictor’s posterior mean and the assumption that its true effect is zero. Therefore, α_j characterizes the implied linear rate of change of information when the effect of any covariate is absent — thus, providing a natural (non-negative) numerical summary of the role of $\tilde{\beta}_j$ in the multivariate distribution. In terms of weightings from the precision matrix, we see the following equivalent representation for the rate of change of the KLD,

$$\alpha_j = \sum_{k \neq j} \sum_{\ell \neq j} c_{k\ell} \lambda_{jk} \lambda_{j\ell},$$

where $c_{k\ell}$ is the corresponding k - ℓ -th element of the matrix $\boldsymbol{\Lambda}_{-j}^{-1}$. As derived in the previous subsection, we may alternatively denote $\alpha_j = \boldsymbol{\theta}_{-j}^\top \boldsymbol{\Lambda}_{-j} \boldsymbol{\theta}_{-j}$, where again $\boldsymbol{\theta}_{-j} = -\boldsymbol{\Lambda}_{-j}^{-1} \boldsymbol{\lambda}_{-j}$ is a $(p-1)$ -dimensional vector and $\boldsymbol{\Lambda}_{-j}$ is the precision matrix of the conditional distribution $p(\tilde{\beta}_{-j} | \tilde{\beta}_j)$. These representations help show that, in the context of normal statistical regression, α_j computes the “variance explained” (i.e. the fitted sum-of-squares) by each covariate \mathbf{x}_j .

The idea of variable selection via entropic shifts also has a key connection to graphical models. Often the goal of graphical models is to investigate if the precision matrix has some off-diagonal series corresponding to an underlying conditional independence structure between covariates (e.g. Carvalho and West, 2007). RATE — a relative distributional centrality measure that assesses importance (or influence) of each variable on the network of relationships reflected in the graph — is greatly affected by the graphical structure resulting from the implied zeros in $\boldsymbol{\Lambda}$. A missing edge between two covariates \mathbf{x}_j and \mathbf{x}_ℓ means that $\lambda_{j\ell} = 0$; hence, limiting the contribution of node ℓ to the overall “network impact factor” of α_j . From the sum defining α_j above, we see that a term related to variables \mathbf{x}_k and \mathbf{x}_ℓ is non-zero only when both λ_{jk} and $\lambda_{j\ell}$ are non-zero. Therefore, the k - ℓ -th summation term is non-zero only for pairs of predictors that are direct neighbors of \mathbf{x}_j in an undirected graph.

4 Results

We now illustrate the utility of using distributional centrality measures for variable selection in Bayesian nonparametric methods through an extensive simulation study and real data analysis. The motivation for each set of examples is to better understand the performance and behavior of RATE under a wide range of underlying data structures. First, we revisit the statistical genetics simulation study introduced in Section

2.4 to help build a stronger intuition about how RATE prioritizes influential covariates. It is during this demonstration where we also explore what happens to the concept of “centrality” when the effects of all known significant predictors are assumed to be absent from the model. Next, we reuse this same simulation design in a high-dimensional association mapping setting to assess the power of our approach. Here, the goal is to show that RATE has the ability to prioritize causal predictors as well as the most commonly used Bayesian and regularization modeling techniques. Finally, we assess the potential of the our approach in an *Arabidopsis thaliana* QTL mapping study consisting of six different phenotypic traits from an F6 Bay-0 \times Shahdara recombinant inbred lines (RILs) population.

4.1 Simulations: Illustrating Distributional Centrality

In this subsection, we revisit the simulation design introduced in Section 2.4 to highlight how distributional centrality measures may be used to prioritize predictors in an association mapping study. To do this, we utilize a simulated matrix \mathbf{X} with $n = 500$ samples and $p = 25$ independently drawn covariates where we now assume that only the last three predictors $p^* = \{23, 24, 25\}$ are causal. Once again, we create continuous outcomes using the following generative linear model: $\mathbf{y} = \mathbf{X}\boldsymbol{\beta} + \mathbf{W}\boldsymbol{\gamma} + \boldsymbol{\varepsilon}$ where $\boldsymbol{\varepsilon} \sim \mathcal{N}(\mathbf{0}, \mathbf{I})$, the additive coefficients are given as $\beta_j \sim \mathcal{U}(0, 1)$ with $\beta_{25} > \beta_{24} > \beta_{23}$, and \mathbf{W} is a matrix that holds all pairwise interactions between the p^* causal predictors with corresponding effect sizes also drawn from a standard uniform distribution or $\gamma_j \sim \mathcal{U}(0, 1)$. Assuming that the covariates make up $V_{\mathbf{x}} = 75\%$ of $V(\mathbf{y})$, we examine three cases for the parameter $\rho = \{0, 0.5, 1\}$. As a brief reminder, ρ represents the proportion of $V_{\mathbf{x}}$ that is contributed by additive effects versus interaction effects. Throughout the rest of this subsection, we focus on results pertaining RATE in the simple linear case with $\rho = 1$ (see Figures 1 and 2). Similar results for other values of ρ can be found in Supporting Information (see Figures S3-S6). Reference results for the unscaled KLD measures can also be found in Supporting Information (see Figures S7-S13).

For each simulated case, we fit a standard GP regression model under a zero mean prior and a Gaussian covariance function using a Gibbs sampler with 10,000 MCMC iterations and model hyper-parameters set to $a = 5$ and $b = 2/5$. During each iterate, a corresponding nonlinear projection is computed as in (6). This results in an approximation of the implied posterior distribution for the effect size analogue. With these conditional draws, we calculate the distribution’s empirical posterior mean, covariance, and precision, and then use the closed form solutions in (10) and (11) to derive a RATE measure for each predictor variable. Figures 1(a) and 2(a) both depict the same illustration of this first order centrality across the 25 covariates. Here, the three known causal variables are colored in blue. As a reference, we also display a red dashed line that is drawn at the level of relative equivalence (i.e. $1/p$). This represents the value for which all predictors are approximately uniform in their centrality or significance. To put this into better context, we provide uniformity checks: (i) the entropic difference Δ according to (12), and (ii) the corresponding empirical ESS estimate as computed in (13). In these first panel figures, we see that RATE accurately determines predictors #23-25 as being the most central to the posterior distribution. More specifically, it accurately identifies variable #25 as being the most associated with the simulated response, followed by covariates #24 and 23 as being second and third, respectively.

To conceptually demonstrate what it means to be central to a distribution, we consider a series of follow-up analyses where we iteratively assume that the effect of the most significantly associated covariate has been nullified from the dataset. We then condition on a reduced margin for the posterior distribution and recompute the RATE measures. The key takeaway here is that, without the effect of the data’s most influential variables, the relative importance of the remaining covariates will continue to shift until each predictor is approximately equal in weight — hence, resembling a uniform distribution. Consider the ongoing example, and assume that we nullify the effect of covariate #25. After recomputing the RATE for every other predictor as the set $\{\text{RATE}(\beta_j | \tilde{\beta}_{25} = 0)\}_{j=1}^{24}$, we see that the variables #24 and #23 are still the most significant according to their second order centrality. Note, however, the importance of the other predictors shift closer to becoming relatively equivalent (see Figure 1(b)). This shift continues when the effects of the remaining causal covariates are also removed successively via $\{\text{RATE}(\tilde{\beta}_j | \tilde{\beta}_{25} = \tilde{\beta}_{24} = 0)\}_{j=1}^{23}$ and $\{\text{RATE}(\tilde{\beta}_j | \tilde{\beta}_{25} = \tilde{\beta}_{24} = \tilde{\beta}_{23} = 0)\}_{j=1}^{22}$ (see Figures 1(c) and 1(d)).

Another key issue is to understand what happens to RATE if one removes the effect of a covariate that is known to be a false positive. Reconsider the ongoing example where, instead of iteratively removing the effect of the most central covariate, we simply nullify predictors #1-3 which we know to be nonsignificant. Figures

2(b)-2(d) illustrate that the three true causal variables (i.e. predictors #23-25) are continuously identified as the most associated predictors. Noticeably, with each passing removal of a nonsignificant covariate, the degree to which the RATE measures begin to look uniform has slowed. We repeat the exact same experiment for the unscaled KLDs, as well as show a plot depicting the behavior of these measures when the outcome is exclusively noise and none of input covariates are considered to have any association (again see Figures S7-S13).

4.2 Simulations: Power Assessment

Next, we assess the power of RATE and its ability to effectively prioritize truly associated covariates under different underlying data structures. To do this, we now consider a high-dimensional version of the previously used simulation scheme with a design matrix containing $n = 500$ samples and $p = 1000$ covariates. As in Section 2.4, we randomly choose $p^* = 30$ causal variables which we classify into two distinct groups: (i) a set of 10 solely additive covariates, and (ii) a set of 20 covariates with both additive and pairwise interaction effects. We then generate continuous outcomes corresponding to simulation scenarios I and II with $V_{\mathbf{x}} = \{0.25, 0.75\}$, and two model generating cases with $\rho = \{0.5, 1\}$.

We compare the GP regression model and our proposed distributional centrality measures to a standard list of Bayesian and regularization modeling techniques. More specifically, these methods include: (a) L1-regularized lasso regression; (b) L2-regularized ridge regression; (c) the combined regularization utilized by the elastic net (Waldmann et al., 2013); (d) a commonly used spike and slab prior model, also commonly known as Bayesian variable selection regression (e.g. Guan and Stephens, 2011), which computes posterior inclusion probabilities (PIPs) for each covariate as a mixture of a point mass at zero and a diffuse normal centered around zero; and (e) a Bayesian linear model with a normal-exponential-gamma (NEG) prior on the effect sizes where posterior probabilities are computed by using a predefined effect-size threshold of interest (Stephens and Balding, 2009). For each Bayesian method, we run a Gibbs sampler for 10,000 MCMC iterations. Regularization approaches were fit by first learning tuning parameter values via 10 fold cross validation.

We investigate the performance of these methodologies on two different data archetypes. The first assumes that each predictor variable is independently simulated, while the second assumes that covariates are simulated according to an underlying correlation structure. Both of these data types aid in the characterization of our centrality approach. The assumption of independent covariates help certain methods avoid problems in deciding what is meant by a “true association” when variables are correlated with one another (Guan and Stephens, 2011). The latter assumption of correlated covariates closely mimics what one may expect to see in real data analyses (e.g. genome-wide association studies; GWASs). As we have previously shown, the computation of RATE depends on the posterior relationship between predictors. Therefore, we would expect our approach to be the more advantageous method when applied to correlated data types.

Once again, all results described in the main text are based on $\rho = 1$, while results for $\rho = 0.5$ can be found in Supporting Information (see Figure S14). We evaluate each method’s ability to accurately identify the $p^* = 30$ causal variables for values of $V_{\mathbf{x}}$. The criteria we use compares the false positive rate (FPR) with the rate at which true covariates are identified for each model (TPR). Figure 3 depicts the proportion of causal predictors discovered after prioritizing all variables in order of their respective significance metrics. Method performance is dependent on two factors: (i) the signal-to-noise ratio in the data generating process, and (ii) the assumed data correlation structure. For example, each of these methods suffer from low power when the signal-to-noise ratio is small and covariates are assumed to be independent (e.g. Figure 3(a) with $V_{\mathbf{x}} = 0.25$). This power increases as the signal-to-noise ratio improves (e.g. Figure 3(b) with $V_{\mathbf{x}} = 0.75$). In this situation, the Bayesian variable selection model with the spike and slab prior proves to be the best method. This is unsurprising as a dataset with independent predictors best suites the spike and slab assumptions where the associations for each variable are individually analyzed.

While the performance of our distributional centrality measures are comparable in the setting of independently drawn covariates, its real advantage becomes apparent in the correlated datasets. Importantly, under this type of data structure scenario, the power of RATE is robust to the presence level of idiosyncratic noise (e.g. Figures 3(c) and 3(d)). More descriptively, in the case of independently generated covariates, solely considering those predictors with RATEs $> 1/p$ identified 39% and 49% of the casual variables in scenarios $V_{\mathbf{x}} = 0.25$ and $V_{\mathbf{x}} = 0.75$, respectively. Comparatively, in the case of covarying predictors, the set

of centrality measures greater than relative equivalence identified 74% and 76% of the associated variables for each respective value of $V_{\mathbf{x}}$. In Figure S15, we show this power to be greater than observing the equivalence of the Bayesian “median probability model” (i.e. PIPs > 0.5 ; Barbieri and Berger, 2004).

These results may be explained by qualitative method assumptions. Each of the competing models that we assess tend to misclassify significant covariates as those that are strongly correlated with a true causal predictor. For example, the L1-regularization conducted by the lasso often selects just one or a few correlated covariates, while the spike and slab prior used within Bayesian variable selection tends to spread the PIPs out among correlated variables (Guan and Stephens, 2011). Here, our centrality variable selection approach has an inherent advantage because it explicitly manipulates properties of the effect size analogue and its joint posterior distribution in order to posit the relative importance of predictors. Again, we stress that this proves to be a particularly relevant feature as the case of correlated variables can be considered a more realistic setting for data analyses.

4.3 Real Data Analysis: RIL QTL Study

We apply our approach to a quantitative trait loci (QTL) association mapping study focused on the characterization of complex traits in *Arabidopsis thaliana*, a small flowering plant native to Eurasia. The specific dataset that we consider comes from the Versailles Arabidopsis Stock Center (<http://publiclines.versailles.inra.fr/page/33>) and has been previously used for evaluating the mapping power of other statistical methods (e.g Demetrashvili et al., 2013). More descriptively, it consists of $n = 420$ F6 plants from a Bay-0 \times Shahdara recombinant inbred lines (RILs) population that were genotyped for $p = 69$ microsatellite markers and phenotyped for twenty different quantitative traits (Loudet et al., 2002). We limit the scope of our analysis to six of these outcomes including: amino acid (AA) content, shoot dry matter (DM), flowering time in long days (FLOLD), nitrate content (NO), nitrogen content percentage (NP), and sulfate content (SO) (see Table S1 in Supporting Information). Note that we consider this particular dataset not only because it presents a variety of quantitative traits, but also because the data contains a mixture of independent and correlated genotypes. These types of genetic architectures have been suggested to manifest different orders of interaction effects (Hemani et al., 2013), and thus this dataset presents a realistic mix between our previously examined simulation scenarios.

For each trait, we provide a summary table which lists all QTL centrality measures that were detected by GP regression via RATE (see Table S2). To contrast the marginal association findings identified by the nonparametric model, we also directly compare results from implementing the spike and slab Bayesian variable selection method and L1-regularized lasso regression (again see Table S2). Figure 4 displays plots of enrichment for a genome wide scan on all six traits according to the RATE enrichment metric. Figure S16 then shows the comparative results for the other two standard association mapping approaches. As a reference in all images, points in color represent genetic markers with significant distributional centrality measures above the line of relative equivalence (i.e. RATEs $> 1/p$). Note that each color corresponds to a different phenotypic trait. In Table 3, we report the number of significant markers that are identified by each method. Once again, these are determined by markers with $\text{RATE}(\hat{\beta}) > 1/p$, $|\hat{\beta}| > 0$, and $\text{PIP}(\beta) > 0.5$, respectively. In the second part of this table, we take the significant markers identified by each model, refit simple linear regressions with them, and report the R^2 of each model fit. Here, we explicitly show that our approach consistently identifies the genetic markers that explain the greatest proportion of variance in all six traits.

Overall, the GP regression model identified a total of 31 of the 69 genetic markers to have at least some moderate association with one of the six analyzed traits. While many of these same variants are identified by the reference lasso and the sparse Bayesian variable selection method (see the latter panel of Table 3), our approach was also able to detect other novel significant markers with potentially biological relevance. For example, in SO, the GP model determined that the top two most central QTL appear on the third chromosome between markers MSAT305754 and ATHCHIB2 (each with RATEs ≈ 0.17). This result is consistent with previous analyses of this trait — where the enrichment of both variants has been linked to the sulfate assimilation gene *ATPS1* (Koprivova et al., 2013) and experimentally validated as factors that are responsible for the variation in sulfate levels (Loudet et al., 2007). Four out of the top six markers with the largest RATEs for this trait have been cited as having a direct relationship with sulfate content and metabolism. These validated findings from previous studies lead us to believe that our results contain true

positives. Lastly, in order to assure confidence in the centrality measures identified by our nonparametric approach, we also display the correlation structure across all of the genotypes for the 420 Bay-0 \times Shahdara RILs (see Figures S17 and S18). Most notably, there appears to be a significant underlying covariance between groups of genetic markers located on different chromosomes. This underlying genetic architecture resembles data analytic situations where our approach is most powered. Complete details of all (potentially) biologically relevant genetic variants discovered across the six traits, as determined by the RATE measure, can be found in Supporting Information.

5 Discussion

In this paper, we proposed a new measure for conducting variable selection in “black box” Bayesian methodologies. While many of these approaches often give notable performance gains, the reasoning behind these results can be difficult to explain and interpret. We discussed how the previously proposed effect size analogue estimate for nonparametric regression enables the prioritization of input variables based on their marginal importance. However, one of the main sources of performance gains in black box modeling is through the underlying covariance between variables. Thus, we introduced our new distributional centrality measure RATE — meant to rank variables based on their influence on the joint distribution with other variables. As we demonstrated with synthetic datasets, our new measure can be used for feature selection, giving state-of-the-art performance in the setting of many correlated predictors. In a QTL association mapping study, RATE allowed us to select better fitting models than linear methods. Here, we were also able to uncover biologically relevant genetic markers by simultaneously taking into account significant covarying interactions when ranking variants based on their relative importance.

RATE is not without its limitations. Perhaps the most noticeable limitation is that the computation of centrality measures scales with the number of features in the input data (see Table S3). An important direction for future work will be to find faster methods to calculate the closed form of the Kullback-Leibler divergence. Perhaps using an approximation to the log-determinant will be helpful here (e.g. Dong et al., 2017). In the current paper, we have not considered the challenges of analyzing large scale studies (e.g. consortium sized efforts in GWASs), but we imagine that subsampling approaches could be of use in these settings (e.g. He and Lin, 2011).

Although our entire method is based on the manipulation of the posterior distribution in Bayesian applications, each of the innovations that we present can be applied in a frequentist setting. The effect size analogue is merely a summary statistic which can be derived after fitting a model. Therefore, one could envision a frequentist setting in which parameter estimation and uncertainty is done using bootstrap, for example. In particular, this would lead to a multivariate normal estimator for the mean and covariance of the effect size analogue. One could then proceed to compute the relative centrality measures with this distribution. The utility of our approach, from this alternative point of view, remains an open question.

The success of black box machine learning-style methods, and their widespread application in scientific and industrial domains, poses a problem of understanding. Asking how a model works is an important question for many current reasons. For example, a “right to explanation” might exist within the European Union’s new and vast data protection regime (Goodman and Flaxman, 2017). Movements such as this will motivate scientists, themselves, to demand explanations. Identifying shortcomings in a model is a key step towards scientific understanding, as well as continuous model expansion (Lakatos, 1980). Moreover, understanding models helps elucidate biases inherent to the datasets on which they are trained. We hope that RATE will contribute towards growing research on all of these important endeavors.

Software Availability

Software for implementing the computation of the RATE measure for variable selection within nonparametric regression methods is carried out in R and Rcpp code, which is freely available at <https://github.com/lorinanthony/RATE>.

Supporting Information

Supporting Information is available for download at <https://github.com/lorinanthony/RATE/tree/master/SI>.

Acknowledgements

LC, SRF, DER, and MW would like to thank Elizabeth R. Hauser (Duke University), Steve Oudot (INRIA Saclay), Sohini Ramachandran (Brown University), and Xiang Zhou (University of Michigan) for useful conversations and suggestions. LC would also like to acknowledge the support of start up funds from Brown University. Any opinions, findings, and conclusions or recommendations expressed in this material are those of the author(s) and do not necessarily reflect the views of any of the funders.

Figures and Tables

Scenario	Terms	True Coefficients	LM	GP	LM+INT	GP+INT
I	\mathbf{x}_1	0.4	0.399 (0.00)	0.396 (0.00)	0.399 (0.00)	0.396 (0.00)
	\mathbf{x}_2	-0.3	-0.300 (0.00)	-0.297 (0.00)	-3.00 (0.00)	-0.297 (0.00)
	\mathbf{x}_3	1.2	1.199 (0.00)	1.188 (0.00)	1.199 (0.00)	1.188 (0.00)
	\mathbf{x}_4	-0.2	-0.199 (0.00)	-0.198 (0.00)	-0.199 (0.00)	-0.198 (0.00)
	$\mathbf{x}_1 \circ \mathbf{x}_2$	0.0	-	-	0.00 (0.00)	0.00 (0.00)
II	\mathbf{x}_1	0.1	0.077 (0.10)	0.076 (0.10)	0.099 (0.00)	0.099 (0.00)
	\mathbf{x}_2	0.2	0.214 (0.12)	0.212 (0.12)	0.200 (0.00)	0.199 (0.00)
	\mathbf{x}_3	0.0	0.001 (0.05)	0.001 (0.05)	-0.000 (0.00)	-0.000 (0.00)
	\mathbf{x}_4	0.0	-0.003 (0.06)	-0.003 (0.06)	0.000 (0.00)	0.000 (0.00)
	$\mathbf{x}_1 \circ \mathbf{x}_2$	1.5	-	-	1.500 (0.00)	1.485 (0.00)

Table 1: Comparison between OLS estimates derived by a standard linear model and the posterior mean of the effect size analogues as computed by the Gaussian process regression method. The second column panel displays the true regression coefficients for the two simulation scenarios. The third column panel displays results while excluding any interaction terms from the design matrix \mathbf{X} . The last group of estimates are computed while considering an augmented design matrix that includes an additional interaction term (INT) between \mathbf{x}_1 and \mathbf{x}_2 , such that $\mathbf{X}^* = [\mathbf{X}; \mathbf{x}_1 \circ \mathbf{x}_2]$ where $\mathbf{x}_1 \circ \mathbf{x}_2 = [\mathbf{x}_{11}\mathbf{x}_{21}, \dots, \mathbf{x}_{1n}\mathbf{x}_{2n}]^\top$. Results are based on 100 replicates in each case with standard errors for each model given in parentheses.

	Scenario	$\rho = 0$		$\rho = 0.5$		$\rho = 1$	
		LM	GP	LM	GP	LM	GP
MSE	I	2.07 (0.3)	0.93 (0.1)	1.79 (0.3)	0.88 (0.1)	2.04 (0.3)	0.93 (0.1)
	II	0.79 (0.1)	0.69 (0.1)	0.88 (0.2)	0.69 (0.1)	0.67 (0.1)	0.67 (0.1)
Opt% _{MSE}	I	0.00	1.00	0.00	1.00	0.00	1.00
	II	0.23	0.77	0.18	0.82	0.55	0.45
r	I	0.20 (0.1)	0.27 (0.1)	0.29 (0.1)	0.37 (0.1)	0.21 (0.1)	0.29 (0.1)
	II	0.65 (0.1)	0.67 (0.0)	0.66 (0.1)	0.70 (0.1)	0.70 (0.1)	0.70 (0.1)
Opt% _{r}	I	0.18	0.82	0.11	0.89	0.13	0.87
	II	0.41	0.59	0.33	0.67	0.51	0.49

Table 2: Comparisons of the out-of-sample predictive mean squared errors (MSE) and predictive correlations (r) for the linear regression model using the standard OLS estimates and the GP regression method using the effect size analogue. Scenarios I and II correspond to signal-to-noise ratios $V_{\mathbf{x}} = \{0.25, 0.75\}$ with control parameter $\rho = \{0, 0.5, 1\}$. Here, $(1 - \rho)$ is used to determine the proportion of signal that is contributed by interaction effects. Results are based on 100 replicates in each case, and the proportion of times for which a method exhibits the lowest MSE or greatest r is denoted as Opt%_{MSE} and Opt% _{r} , respectively. Values in bold represent the approach with the best (and most robust) performance. Standard errors for each model are given in the parentheses.

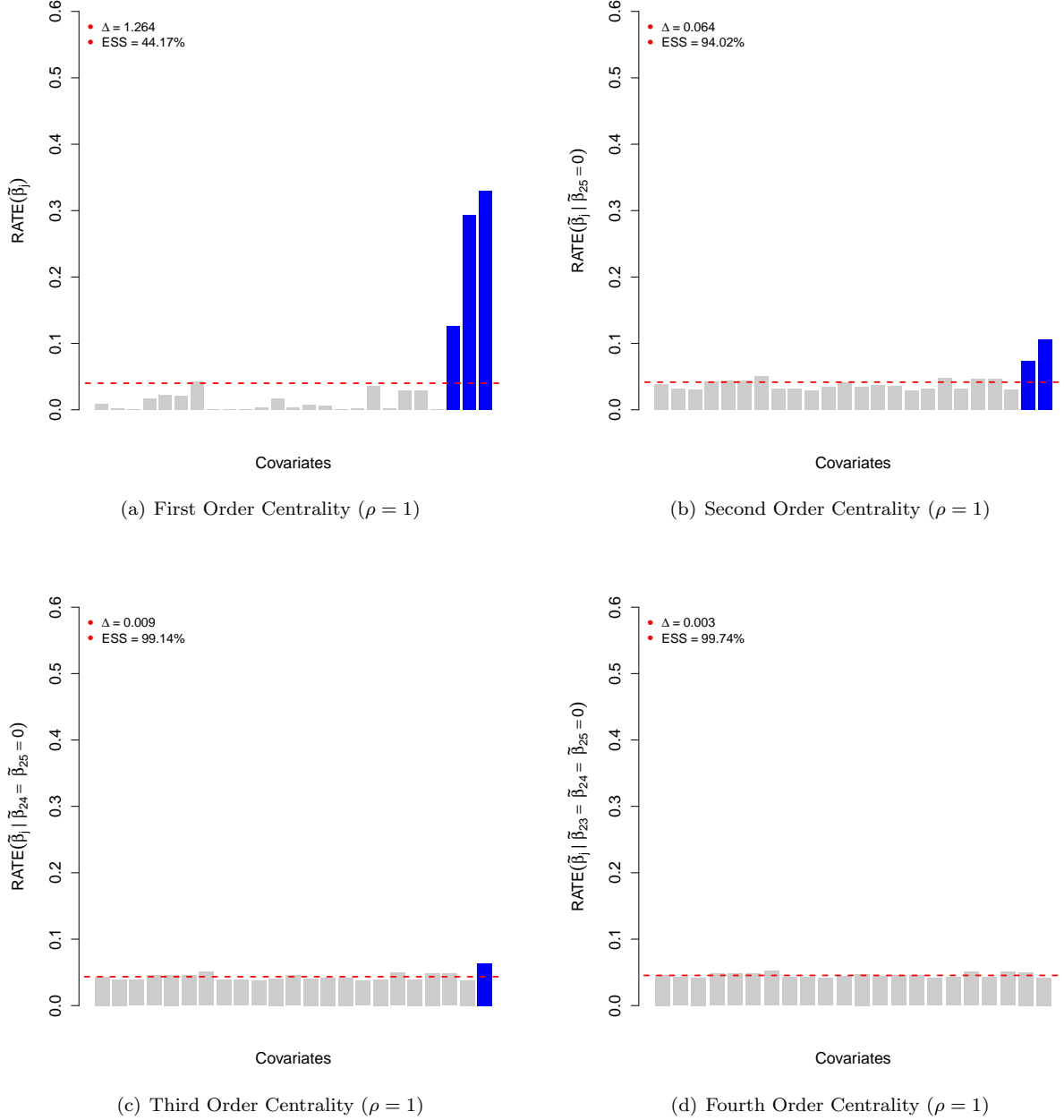


Figure 1: Demonstrating different orders of distributional centrality via RATE measures. Data are simulated such that only the effects of the last three covariates $p^* = \{23, 24, 25\}$ (blue) are nonzero with $\beta_{25} > \beta_{24} > \beta_{23}$. Outcomes are generated using a signal-to-noise ratio $V_{\mathbf{x}} = 0.75$ with $\rho = 1$. Here, $(1 - \rho)$ is used to determine the proportion of signal that is contributed by interaction effects. The x-axis of each figure shows the index of the different predictors, while the y-axis gives their relative centrality measures. The red dashed line is drawn at the level of relative equivalence (i.e. $1/p$). Figure (a) depicts the first order centrality across all predictors. Figures (b)–(d) illustrate scenarios where the most significantly associated covariates are iteratively nullified. These figures present results for the sets: (b) $\{\text{RATE}(\tilde{\beta}_j | \tilde{\beta}_{25} = 0)\}_{j=1}^{24}$; (c) $\{\text{RATE}(\tilde{\beta}_j | \tilde{\beta}_{25} = \tilde{\beta}_{24} = 0)\}_{j=1}^{23}$; and (d) $\{\text{RATE}(\tilde{\beta}_j | \tilde{\beta}_{25} = \tilde{\beta}_{24} = \tilde{\beta}_{23} = 0)\}_{j=1}^{22}$, respectively. We also report values representing the degree to which the landscape of RATEs begin to look uniform: (i) the entropic difference Δ , and (ii) the corresponding empirical ESS estimate.

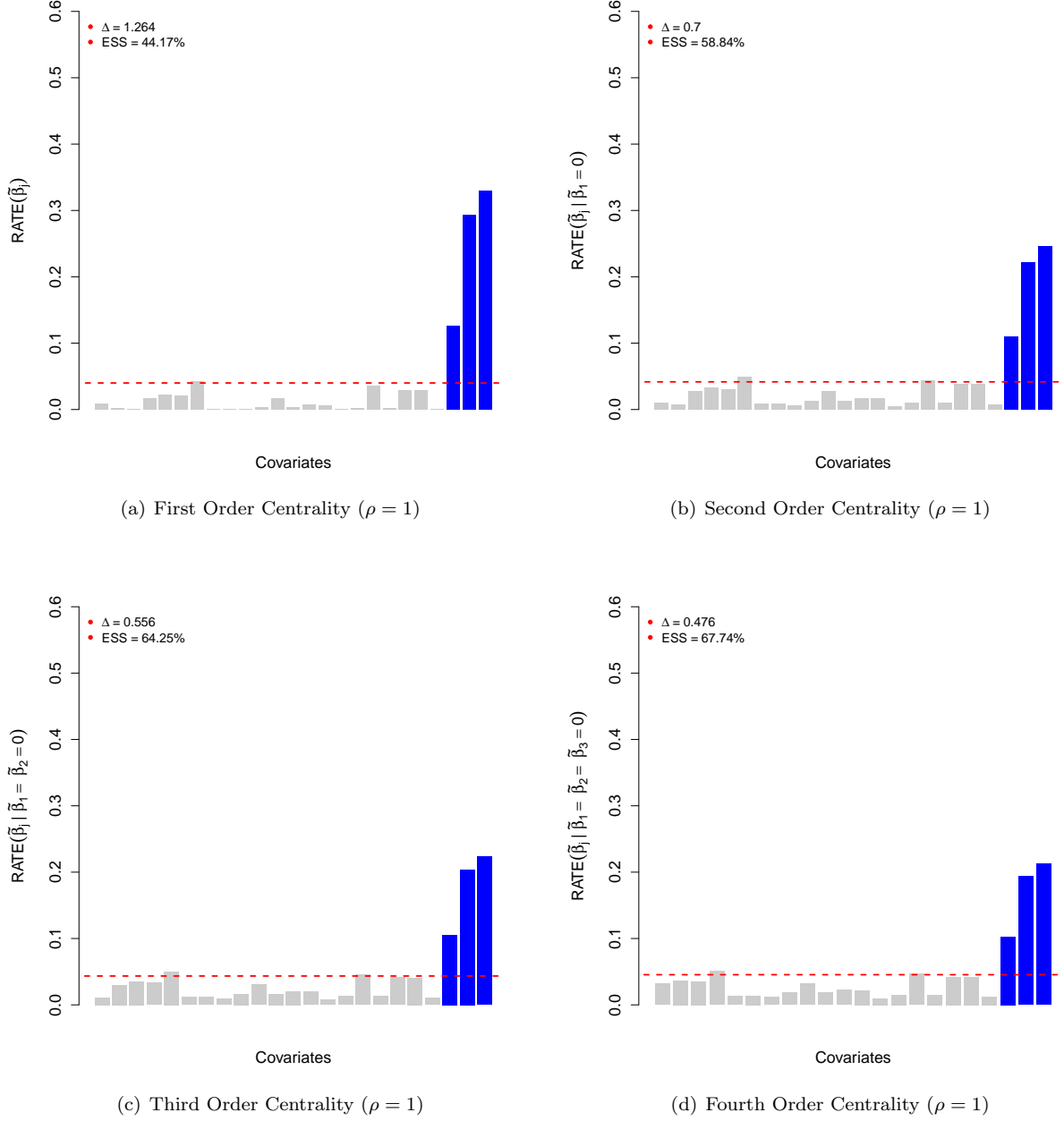
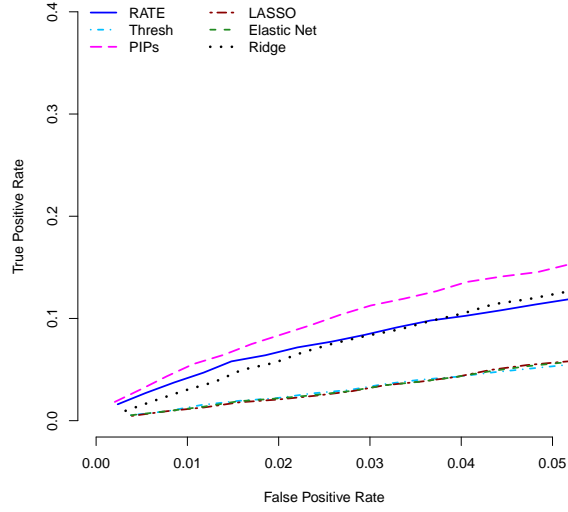
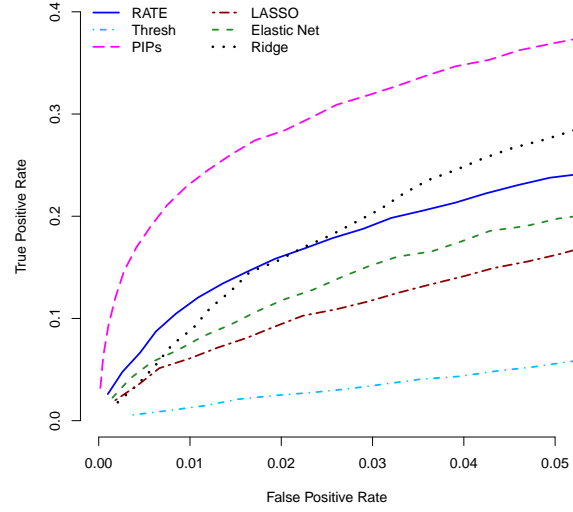


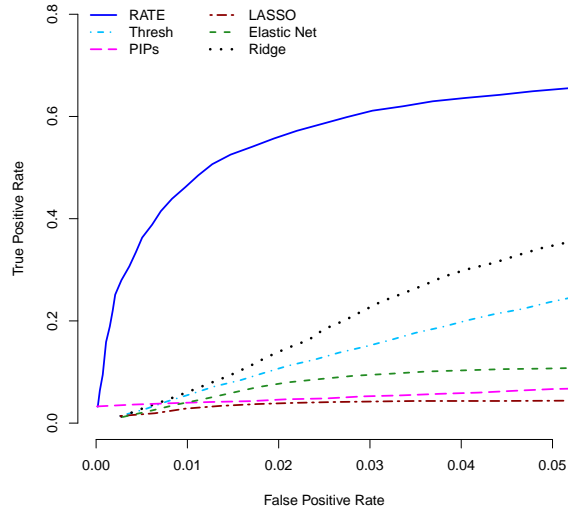
Figure 2: Distributional centrality and false positives with RATE measures. Data are simulated such that only the effects of the last three covariates $p^* = \{23, 24, 25\}$ (blue) are nonzero with $\beta_{25} > \beta_{24} > \beta_{23}$. Outcomes are generated using a signal-to-noise ratio $V_{\mathbf{x}} = 0.75$ with $\rho = 1$. Here, $(1 - \rho)$ is used to determine the proportion of signal that is contributed by interaction effects. The x-axis of each figure shows the index of the different predictors, while the y-axis gives their relative centrality measures. The red dashed line is drawn at the level of relative equivalence (i.e. $1/p$). Figure (a) depicts the first order centrality across all predictors. Figures (b)-(d) illustrate scenarios where known nonsignificant predictors #1-3 are iteratively nullified. These figures present results for the sets: (b) $\{\text{RATE}(\tilde{\beta}_j | \tilde{\beta}_1 = 0)\}_{j \neq 1}$; (c) $\{\text{RATE}(\tilde{\beta}_j | \tilde{\beta}_1 = \tilde{\beta}_2 = 0)\}_{j \neq (1,2)}$; and (d) $\{\text{RATE}(\tilde{\beta}_j | \tilde{\beta}_1 = \tilde{\beta}_2 = \tilde{\beta}_3 = 0)\}_{j \neq (1,2,3)}$, respectively. We also report values representing the degree to which the landscape of RATEs begin to look uniform: (i) the entropic difference Δ , and (ii) the corresponding empirical ESS estimate.



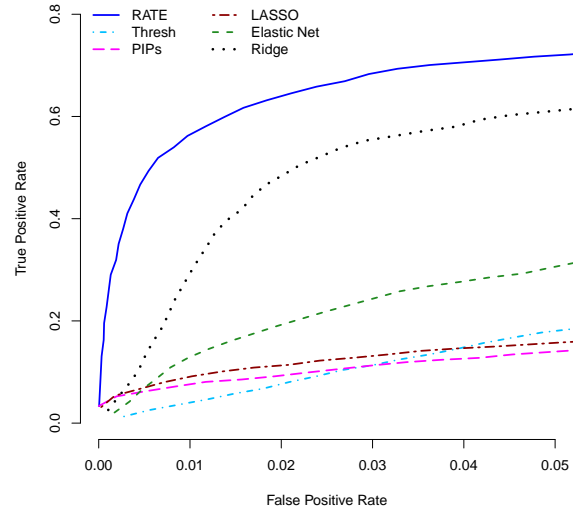
(a) Independent Predictors ($V_{\mathbf{x}} = 0.25$; $\rho = 1$)



(b) Independent Predictors ($V_{\mathbf{x}} = 0.75$; $\rho = 1$)



(c) Correlated Predictors ($V_{\mathbf{x}} = 0.25$; $\rho = 1$)



(d) Correlated Predictors ($V_{\mathbf{x}} = 0.75$; $\rho = 1$)

Figure 3: Power analysis for prioritizing causal covariates. We compare the association mapping ability of our nonparametric centrality measures (RATEs) to the standard significance metrics provided by ridge regression, lasso regression, the elastic net, Bayesian variable selection method with a spike and slab prior (PIPs), and a Bayesian linear model with a normal-exponential-gamma prior and thresholded effect sizes (Thresh). Figures (a) and (b) display results when data is simulated using independent predictors; while Figures (c) and (d) correspond to results under correlated predictors. In either case, outcomes are generated using a signal-to-noise ratio $V_{\mathbf{x}} = \{0.25, 0.75\}$ with $\rho = 1$. Here, $(1 - \rho)$ is used to determine the proportion of signal that is contributed by interaction effects. The x-axis shows the false positive rate, while the y-axis gives the rate at which true causal variables were identified. Results are based on 100 replicates in each case.

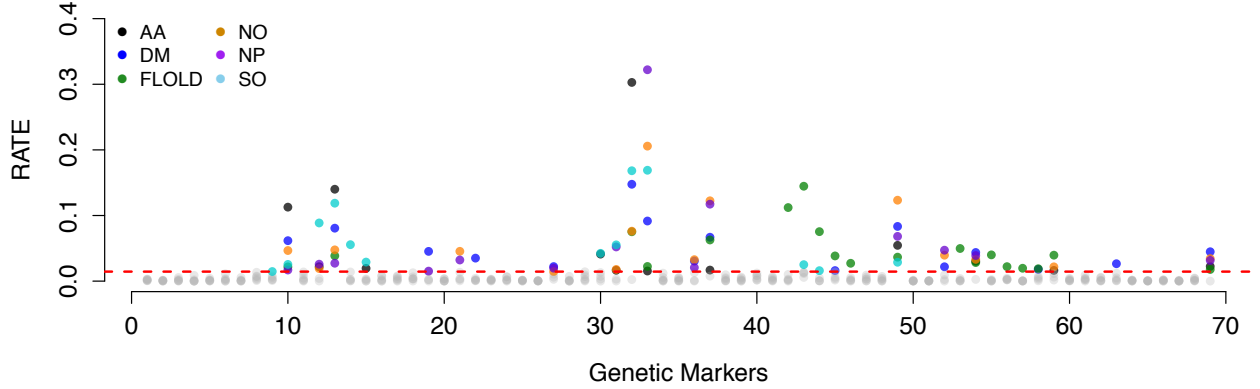


Figure 4: Genetic map wide scan on all six traits analyzed in the *Arabidopsis thaliana* QTL mapping study. The six traits analyzed include: amino acid (AA) content, shoot dry matter (DM), flowering time in long days (FLOLD), nitrate content (NO), nitrogen content percentage (NP), and sulfate content (SO). For each phenotype, the relative centrality measures (RATE) for microsatellite genetic markers are plotted in order of their positions along the genome. Points in color represent genetic markers with significant distributional centrality measures above the line of relative equivalence (i.e. RATEs $> 1/p$). Note that each color corresponds to a different phenotypic trait.

Category	Method	Phenotypic Traits					
		AA	DM	FLOLD	NO	NP	SO
# Sig. Markers	RATE	13	16	19	15	14	13
	Lasso	12	11	14	9	14	28
	PIPs	10	10	4	8	8	14
R^2 of Sig. Model	RATE	0.629	0.548	0.654	0.522	0.535	0.867
	Lasso	0.145	0.095	0.080	0.034	0.031	0.605
	PIPs	0.499	0.415	0.409	0.282	0.353	0.802
% Overlap	Lasso \subseteq RATE	25%	27%	50%	33%	14%	39%
	PIPs \subseteq RATE	30%	0%	75%	38%	13%	29%

Table 3: A summary table comparing the genetic markers discovered in the *Arabidopsis thaliana* QTL mapping study. The six traits analyzed include: amino acid (AA) content, shoot dry matter (DM), flowering time in long days (FLOLD), nitrate content (NO), nitrogen content percentage (NP), and sulfate content (SO). Here, we use the proposed nonparametric association mapping approach with the relative centrality measures (RATEs). Results for the standard lasso regression and Bayesian variable selection method with a spike and slab prior (PIPs) are also considered. The first part of the table displays the number of significant markers that are identified by each method. These are determined by markers with $\text{RATE}(\hat{\beta}) > 1/p$, $|\hat{\beta}| > 0$, and $\text{PIP}(\beta) > 0.5$, respectively. The second part of this table takes these significant markers identified by each model, refits a simple linear model with them, and reports the R^2 of the model fit. Values in bold represent the approach that identified variables that explain the greatest proportion of the variance in a given trait. The last section of this table describes the percent overlap between the markers found using RATE and those detected with the competing methods.

References

- Alaa, A. M. and M. van der Schaar (2017). Bayesian nonparametric causal inference: Information rates and learning algorithms. *arXiv:1712.08914*.
- Barbieri, M. M. and J. O. Berger (2004). Optimal predictive model selection. *The Annals of Statistics* 32(3), 870–897.
- Carvalho, C. M., N. G. Polson, and J. G. Scott (2010). The horseshoe estimator for sparse signals. *Biometrika* 97(2), 465–480.
- Carvalho, C. M. and M. West (2007). Dynamic matrix-variate graphical models. *Bayesian Anal.* 2(1), 69–97.
- Chaudhuri, A., D. Kakde, C. Sadek, L. Gonzalez, and S. Kong (2017). The mean and median criterion for automatic kernel bandwidth selection for support vector data description. *arXiv:1708.05106*.
- Chipman, H. A., E. I. George, and R. E. McCulloch (2010). Bart: Bayesian additive regression trees. *The Annals of Applied Statistics* 4(1), 266–298.
- Cotter, A., J. Keshet, and N. Srebro (2011). Explicit approximations of the Gaussian kernel. *arXiv:1109.4603*.
- Crawford, L., K. C. Wood, X. Zhou, and S. Mukherjee (2017). Bayesian approximate kernel regression with variable selection. *Journal of the American Statistical Association*. Available online from <https://doi.org/10.1080/01621459.2017.1361830>.
- Demetrashvili, N., E. Van den Heuvel, and E. Wit (2013). Probability genotype imputation method and integrated weighted lasso for QTL identification. *BMC genetics* 14, 125.
- Dong, K., D. Eriksson, H. Nickisch, D. Bindel, and A. G. Wilson (2017). Scalable log determinants for Gaussian process kernel learning. *Neural Information Processing Systems (NIPS)* 30, 6330–6340.
- Drineas, P. and M. W. Mahoney (2005). On the Nyström method for approximating a Gram matrix for improved kernel-based learning. *J. Mach. Learn. Res.* 6, 2153–2175.
- Fasshauer, G. and M. McCourt (2016). *Kernel-based Approximation Methods using Matlab*. World Scientific.
- Goodman, B. and S. Flaxman (2017). European Union regulations on algorithmic decision making and a “right to explanation”. *AI Magazine* 38(3), 50–58.
- Goutis, C. and C. P. Robert (1998). Model choice in generalised linear models: A Bayesian approach via Kullback-Leibler projections. *Biometrika* 85(1), 29–37.
- Gruber, L. F. and M. West (2016). GPU-accelerated Bayesian learning in simultaneous graphical dynamic linear models. *Bayesian Analysis* 11, 125–149.
- Gruber, L. F. and M. West (2017). Bayesian forecasting and scalable multivariate volatility analysis using simultaneous graphical dynamic linear models. *Econometrics and Statistics* 3, 3–22. *arXiv:1606.08291*.
- Guan, Y. and M. Stephens (2011). Bayesian variable selection regression for genome-wide association studies and other large-scale problems. *Ann. Appl. Stat.* 5(3), 1780–1815.
- He, Q. and D.-Y. Lin (2011). A variable selection method for genome-wide association studies. *Bioinformatics* 27(1), 1–8.
- Hemani, G., S. Knott, and C. Haley (2013). An evolutionary perspective on epistasis and the missing heritability. *PLoS Genet* 9(2), e1003295.
- Hemani, G., K. Shakhbazov, H.-J. Westra, T. Esko, A. K. Henders, A. F. McRae, J. Yang, G. Gibson, N. G. Martin, A. Metspalu, L. Franke, G. W. Montgomery, P. M. Visscher, and J. E. Powell (2014). Detection and replication of epistasis influencing transcription in humans. *Nature* 508(7495), 249–253.

- Hill, W. G., M. E. Goddard, and P. M. Visscher (2008). Data and theory point to mainly additive genetic variance for complex traits. *PLoS Genet* 4(2), e1000008.
- Horn, T., T. Sandmann, B. Fischer, E. Axelsson, W. Huber, and M. Boutros (2011). Mapping of signaling networks through synthetic genetic interaction analysis by RNAi. *Nat Meth* 8(4), 341–346.
- Howard, R., A. L. Carriquiry, and W. D. Beavis (2014). Parametric and nonparametric statistical methods for genomic selection of traits with additive and epistatic genetic architectures. *G3: Genes, Genomes, Genetics* 4(6), 1027–1046.
- Jiang, Y. and J. C. Reif (2015). Modeling epistasis in genomic selection. *Genetics* 201, 759–768.
- Kolmogorov, A. N. and Y. A. Rozanov (1960). On strong mixing conditions for stationary Gaussian processes. *Theory of Probability & Its Applications* 5(2), 204–208.
- Koprivova, A., M. Giovannetti, P. Baraniecka, B.-R. Lee, C. Grondin, O. Loudet, and S. Kopriva (2013). Natural variation in the ATPS1 isoform of ATP sulfurylase contributes to the control of sulfate levels in Arabidopsis. *Plant Physiology* 163(3), 1133–1141.
- Lakatos, I. (1980). *The Methodology of Scientific Research Programmes: Volume 1: Philosophical Papers*, Volume 1. Cambridge University Press.
- Liang, F., R. Paulo, G. Molina, M. A. Clyde, and J. O. Berger (2008). Mixtures of g -priors for Bayesian variable selection. *Journal of the American Statistical Association* 103(481), 410–423.
- Lim, C. and B. Yu (2016). Estimation stability with cross-validation (escv). *Journal of Computational and Graphical Statistics* 25(2), 464–492.
- Lin, L., C. Chan, and M. West (2016). Discriminative variable subsets in Bayesian classification with mixture models, with application in flow cytometry studies. *Biostatistics* 17(1), 40–53.
- Loudet, O., S. Chaillou, C. Camilleri, D. Bouchez, and F. Daniel-Vedele (2002). Bay-0 \times Shahdara recombinant inbred line population: A powerful tool for the genetic dissection of complex traits in Arabidopsis. *Theoretical and Applied Genetics* 104(6), 1173–1184.
- Loudet, O., V. Saliba-Colombani, C. Camilleri, F. Calenge, V. Gaudon, A. Koprivova, K. A. North, S. Kopriva, and F. Daniel-Vedele (2007). Natural variation for sulfate content in *Arabidopsis thaliana* is highly controlled by APR2. *Nature Genetics* 39, 896 EP.
- Mackay, T. F. C. (2014). Epistasis and quantitative traits: Using model organisms to study gene-gene interactions. *Nat Rev Genet* 15(1), 22–33.
- Mathai, A. M. and S. B. Provost (1992). *Quadratic Forms in Random Variables*. Taylor & Francis.
- Mercer, J. (1909). Functions of positive and negative type and their connection with the theory of integral equations. *Philosophical Transactions of the Royal Society, London A* 209, 415–446.
- Piironen, J. and A. Vehtari (2016). Projection predictive model selection for Gaussian processes. In *Machine Learning for Signal Processing (MLSP), 2016 IEEE 26th International Workshop on*, pp. 1–6. IEEE.
- Piironen, J. and A. Vehtari (2017). Comparison of Bayesian predictive methods for model selection. *Statistics and Computing* 27(3), 711–735.
- Pillai, N. S., Q. Wu, F. Liang, S. Mukherjee, and R. Wolpert (2007). Characterizing the function space for Bayesian kernel models. *Journal of Machine Learning Research* 8, 1769–1797.
- Rahimi, A. and B. Recht (2007). Random features for large-scale kernel machines. *Neural Information Processing Systems (NIPS)* 3(4), 5.
- Rasmussen, C. E. and C. K. I. Williams (2006). *Gaussian Processes for Machine Learning*. Cambridge, MA: MIT Press.

- Richard, M. D. and R. P. Lippmann (1991). Neural network classifiers estimate Bayesian *a posteriori* probabilities. *Neural computation* 3(4), 461–483.
- Schölkopf, B., R. Herbrich, and A. J. Smola (2001). A generalized representer theorem. In *Proceedings of the 14th Annual Conference on Computational Learning Theory and 5th European Conference on Computational Learning Theory*, London, UK, UK, pp. 416–426. Springer-Verlag.
- Smith, A., P. A. Naik, and C.-L. Tsai (2006). Markov-switching model selection using Kullback–Leibler divergence. *Journal of Econometrics* 134(2), 553–577.
- Stephens, M. and D. J. Balding (2009). Bayesian statistical methods for genetic association studies. *Nature Reviews Genetics* 10, 681–690.
- Tan, S., R. Caruana, G. Hooker, and Y. Lou (2017). Detecting bias in black-box models using transparent model distillation. arXiv:1710.06169.
- Wahba, G. (1990). *Splines Models for Observational Data*, Volume 59 of *Series in Applied Mathematics*. Philadelphia, PA: SIAM.
- Waldmann, P., G. Mészáros, B. Gredler, C. Fürst, and J. Sölkner (2013). Evaluation of the lasso and the elastic net in genome-wide association studies. *Frontiers in Genetics* 4, 270.
- Woo, J. H., Y. Shimoni, W. S. Yang, P. Subramaniam, A. Iyer, P. Nicoletti, M. Rodríguez Martínez, G. López, M. Mattioli, R. Realubit, C. Karan, B. R. Stockwell, M. Bansal, and A. Califano (2015). Elucidating compound mechanism of action by network perturbation analysis. *Cell* 162(2), 441–451.
- Wood, A. R., M. A. Tuke, M. A. Nalls, D. G. Hernandez, S. Bandinelli, A. B. Singleton, D. Melzer, L. Ferrucci, T. M. Frayling, and M. N. Weedon (2014). Another explanation for apparent epistasis. *Nature* 514(7520), E3–E5.
- Zhang, Z., G. Dai, and M. I. Jordan (2011). Bayesian generalized kernel mixed models. *Journal of Machine Learning Research* 12, 111–139.